Applied Geochemistry 101 (2019) 160–169

Contents lists available at ScienceDirect

Applied Geochemistry

journal homepage: www.elsevier.com/locate/apgeochem

Long-term stability of dithionite in alkaline anaerobic aqueous solution

Katherine Telfeyan*, Artas A. Migdisov, Sachin Pandey, Velimir V. Vesselinov, Paul W. Reimus

Earth and Environmental Sciences Division, Los Alamos National Laboratory, Los Alamos, NM, 87545, United States

ARTICLE INFO

Editorial handling by Eric M Pierce

Keywords:
Dithionite
Sulfur redox chemistry
Hydrolysis reaction
In-situ redox manipulation

ABSTRACT

Closed-system experiments were conducted to investigate the decomposition of sodium dithionite in aqueous solutions under varying pH and starting concentrations to simulate the deployment of dithionite as an in-situ redox barrier. Co-determination of dithionite and its degradation products was conducted using UV–Vis spectrometry, iodometric titration, and ion chromatography. In unbuffered solutions, dithionite reacted rapidly, whereas in near-neutral solutions (pH ~7), it persisted for ~ 50 days and in alkaline solution (pH ~9.5) for > 100 days. These are the longest lifetimes reported to date, which we attribute to not only excluding oxygen but also preventing outgassing of H_2S. Thoroughly constraining the reaction products has led to the following hypothesized reaction:

$$4\ S_2O_4^{2-} + H_2O \rightarrow HS^- + SO_3^{2-} + 2\ SO_4^{2-} + S_4O_6^{2-} + H^+$$

which represents relatively rapid degradation at near-neutral pH values. At the more alkaline pH, and over longer time scales, the reaction is best represented by:

$$3\ S_2O_4^{2-} + 3\ H_2O \rightarrow 2HS^- + SO_3^{2-} + 3\ SO_4^{2-} + 4\ H^+$$

the following kinetic rate law was developed for the pH range studied:

$$\frac{dC_i}{dt} = S_i 10^{-4.81}\{H^+\}^{0.24}\{S_2O_4^{2-}\},$$

where $\frac{dC_i}{dt}$ is the rate of change of the i^{th} chemical component in the simplified equation (mole $L^{-1}\ s^{-1}$) and S_i is the stoichiometric coefficient of the ith chemical. The kinetic rate law was used to calculate a pseudo first order half-life of 10.7 days for near-neutral pH and 33.6 days for alkaline pH. This work implies that if hydrogen sulfide is contained within the system, such as in the case of a confined aquifer below the water table, dithionite decomposes more slowly in alkaline aqueous solution than previously thought, and thus it may be more cost-effectively distributed in aquifers than has been previously assumed.

1. Introduction

Sulfur is among the most important elements controlling redox equilibria in natural aqueous systems, including high temperature submagmatic fluids, geothermal waters, acid-sulfate pools, as well as low temperature systems such as wetlands and geochemical systems artificially created in subsurface aquifers during remediation of contaminated horizons (Luther and Church, 1998; Migdisov and Bychkov, 1998; Fruchter et al., 1999; Burton et al., 2011; Kassalainen and Stefánsson, 2011a,b; Couture et al., 2016). Complexity of the response of sulfur equilibria to changing redox conditions and, thus, its ability to fine-tune redox conditions of geochemical systems, is due to a large number of oxidation states and intermediate species that this element can form in aqueous solutions. The transfer of 8 electrons during oxidation of sulfide to sulfate produces species such as, SO_3^{2-}, $S_2O_3^{2-}$, S_8°, polysulfides, and polythionates, with the relative proportions depending upon the oxidation state and pH of the system (Kassalainen and Stefánsson, 2011a,b). Quantitative understanding of their relationships is therefore crucial for constraining geochemical controls of these systems and predicting geochemical behavior of redox-sensitive elements. Considerable work has focused on characterizing the S speciation in environments such as hydrothermal waters (Xu et al., 1998; Kassalainen and Stefánsson, 2011a,b), and crater lakes (Casas et al., 2016; Takano, 1987; Takano and Watanuki, 1990; Takano et al., 1994a,b). Changes in sulfur species distribution have also been used as a tool for monitoring volcanic activity and fault geometry (Casas et al., 2016; Takano, 1987; Takano and Watanuki, 1990; Takano et al., 1994a,b). Many of these intermediate redox species, however, are metastable, and thus their distribution depends largely on kinetics, making accurate quantitative determination difficult (Kassalainen and Stefánsson, 2011a,b; Williamson and Rimstidt, 1992).

From the point of view of environmental geochemistry, a

* Corresponding author.
E-mail addresses: ktelfeyan@lanl.gov, ktelfeya@tulane.edu (K. Telfeyan).

https://doi.org/10.1016/j.apgeochem.2018.12.015
Received 25 December 2017; Received in revised form 9 December 2018; Accepted 10 December 2018
Available online 11 December 2018
0883-2927/ Published by Elsevier Ltd.

particularly important intermediate, sodium dithionite, has proven invaluable in environmental remediation for in-situ redox treatment of contaminated groundwater as a strong reducing agent (Istok et al., 1999; Amonette et al., 1994). Dithionite reduces structural ferric iron in iron-bearing minerals according to

$$S_2O_4^{2-} + 2Fe(III)_{(s)} + 2H_2O \rightarrow 2SO_3^{2-} + 2Fe(II)_{(s)} + 4H^+ \quad (1)$$

forming a permeable treatment zone, capable of reducing and immobilizing certain redox-sensitive elements (Istok et al., 1999). Dithionite has been successfully used to treat plumes of Cr(VI) (Istok et al., 1999; Fruchter et al., 1999; Amonette et al., 1994; Ludwig et al., 2007), perchloroethylene (Nzengung et al., 2001), trichloroethylene (Szecsody et al., 2004), and explosive contaminants (Boparai et al., 2008). Additionally, dithionite has been shown to extend the lifetime of nanoscale zero-valent iron also used in contaminant removal (Xie and Cwiertny, 2010). Yet, dithionite is unstable, and the concentration of dithionite itself and its degradation products changes with time and is highly dependent on the aquifer conditions (Holman and Bennett, 1994). Geochemical modelling of the systems on which this remediant has been applied and evaluation of the longevity of its effects therefore require quantitative knowledge of its degradation rate, stoichiometry of its decomposition, and variability of these properties with changing aquifer conditions.

Unfortunately, the data currently available in the literature on the lifetime of dithionite and its decomposition products are highly scattered (Table 1). One of the factors influencing determined decomposition rates of dithionite and, thus, partially explaining scattering of the data, is the pH at which experiments were performed. It has been consistently shown since the initial work in the early 1900s that decomposition of dithionite greatly accelerates when pH decreases. The greater decomposition under acidic conditions is attributed to a greater decomposition rate of the protonated species $HS_2O_4^-$ or $H_2S_2O_4$ relative to the unprotonated $S_2O_4^{2-}$, which is predominant in alkaline solutions (Lister and Garvie, 1959). Therefore, dithionite in unbuffered or acidic solution is impractical as a treatment option, and all previous deployments have added a basic buffer to extend its lifetime. For example, during deployment of dithionite to treat a Cr(VI) plume, Istok et al. (1999) buffered the dithionite solution with a CO_3^{2-}/HCO_3^- solution to pH ~11. Dithionite decomposition is slower in anaerobic, alkaline solutions and reportedly follows pseudo-first order decay (Ammonette et al., 1994; Lister and Garvie, 1959) or half-order decay in excess alkali (Kilroy, 1980). However, even in alkaline solution, the data on dithionite decomposition is inconsistent (Table 1). Previously reported experimental rate constants vary from $4.5{\cdot}10^{-4}$ min^{-1} (88.5 °C) (Lister and Garvie, 1959), 0.015 $M^{0.5}min^{-1}$ (82 °C) (Kilroy, 1980), and $4.8–8.5{\cdot}10^{-5}$ min^{-1} (varying dithionite concentrations; Amonette et al., 1994). At pH 13, Münchow and Steudel (1994) observed no noticeable loss of dithionite from anaerobic solution for the duration of their study (4 days), but Amonette et al. (1994) measured dithionite after ~ 2 weeks. One explanation for such discrepancies is the extent of containment of the experimental solutions. Indeed, if the suggestion of the formation of H_2S as the decomposition product of dithionite is correct (Wayman and Lem, 1970), poor containment of the system should inevitably lead to losses of this component from the solution and acceleration of the decomposition of dithionite. These losses can potentially occur as degassing of the solution due to formation of H_2S gas (even in inert gas-filled compartments, such as gloveboxes), or, if solutions are not protected from the atmosphere, due to oxidation of H_2S by atmospheric oxygen. It should be noted that the majority of the experimental studies referred to above prevented oxygen intrusion but did not take any special precaution to address the outgassing of H_2S, and therefore they may have underestimated the dithionite lifetimes. Moreover, the vast majority of the studies available in the literature on the decomposition of dithionite have been performed for durations not exceeding 2 weeks, primarily due to quick decomposition of dithionite. However, if this quick decomposition is caused by the effects discussed above (e.g., poor containment of the solutions), these data can be misleading for modelling dithionite behavior in anoxic aquifers in which confined conditions with respect to gas exchange often exist and in which the lifetime of dithionite can potentially be significantly longer. Even in oxic aquifers, anoxic conditions will eventually prevail in the immediate vicinity of an injection well because the injected dithionite will consume all available oxidants near the well. If dithionite is continuously injected under these conditions, the distance that it can ultimately be pushed into an aquifer will be dictated by its anaerobic decomposition rate in the presence of aqueous phase reaction products. The goal of our study is therefore to investigate the stability of dithionite in well-contained systems and, if it is found that containment

Table 1
Summary of previous studies' experimental conditions and results.

Reference	Experimental Conditions	Results
Lister and Garvie (1959)	T = 88 °C; N_2 atmosphere; $[S_2O_4^{2-}]$ = 0.034–0.142 M; Buffer: 0.05–0.2 M NaOH	$k = 4.5{\cdot}10^{-4}$ min^{-1}
Rinker et al. (1965)	T = 60–80 °C; $[S_2O_4^{2-}]$ = 0.0055–0.0115 M; pH = 4–7 (KH_2PO_4 and NaOH)	$R_{induction} = k_c[S_2O_4^{2-}]_T^{3/2}{\cdot}[H^+]^{1/2}$ $k_c = 1.3{\cdot}10^8{\cdot}e^{-12000/RT}$ L mol^{-1} sec^{-1}
Spencer (1967)	T = 15–35 °C $[S_2O_4^{2-}]$ = 0.015–0.2 M in solution of HSO_3^-, SO_3^{2-}, NaCl (pH 5.2)	First-order decay Decomposition products: trithionate, thiosulfate
Burlamacchi et al. (1969)	T = 60–90 °C $[S_2O_4^{2-}]$ = 0.067, 0.125, 0.25 M; pH = 6 (phosphate buffer)	$-d[S_2O_4^{2-}]/dt = k'[S_2O_4^{2-}][HSO_3^-]$ $k' = 0.57–7.8{\cdot}10^3$ L mol^{-1} s^{-1}
Lem and Wayman (1970)	T = 23 °C; Ar atmosphere; $[S_2O_4^{2-}]$ = 1, 2, 5, $10{\cdot}10^{-3}$ M; pH range: 3.5, 4, 4.5, 5 (Buffers: acetate, sodium hydrogen phosphate-citric acid)	$-dC/dt = k_1[H^+]C + k_2[H^+]C(Co-C)$ k_1: $1.67{\cdot}10^{-1}$ L $mol^{-1}s^{-1}$ $k_2 = 5.83{\cdot}10^3$ L^2 $mole^{-2}$ s^{-1}
Kilroy (1980)	T = 82 °C; Ar atmosphere; $[S_2O_4^{2-}]$ = 0.02–0.08 M; Buffer: NaOH	$k = 0.014–0.018$ $(mol/L)^{0.5}$ min^{-1}
Holman and Bennett (1994)	T = 42–88.5 °C; N_2 purged Excess Bisulfite pH: mildly acidic	$d[S_2O_4^{2-}]/dt = -k_1[S_2O_4^{2-}][HSO_3^-]-k_2[S_2O_4^{2-}]^{0.5}[HSO_3^-][S_3O_6^{2-}]$ $k_1 = (3.1 \pm 0.3{\cdot}10^2\ M^{-1}s^{-1}{\cdot}T{\cdot}\exp(-(54.3 \pm 5)/RT)$ $k_2 = (1.67 \pm 0.2{\cdot}10^7\ M^{-3/2}s^{-1}T{\cdot}\exp(-(78.4 \pm 7)/RT)$
Münchow and Steudel (1994)	T = 20 °C; $[S_2O_4^{2-}]$ = 0.0214 M; pH: 5.7, 13	Reaction products: thiosulfate, sulfite Dithionite in alkaline solution persists (Experiments not exceeding 2 h)
Amonette et al. (1994)	T = 30 °C; Ar (95%), H_2(4%); $[S_2O_4^{2-}]$ = 0.002, 0.013, 0.06 M; $CaCO_3$ buffer	0.06 M: $t_{1/2}$ = 135 h; $k_{app} = 8.5{\cdot}10^{-5}$ min^{-1} 0.002 M: $t_{1/2}$ = 243 h; $k_{app} = 4.8{\cdot}10^{-5}$ min^{-1}
de Carvalho and Schwedt (2001)	$[S_2O_4^{2-}]$ = 0.0065 M Background solutions of formaldehyde, NaOH, HMTA in glyceral and water, diammonium hydrogen phosphate/ammonium hydroxide, Triton X-100	Major reaction products: sulfite thiosulfate Minor reaction products: sulfide, elemental S

increases the lifetime of dithionite, to expand the time range up to months. This study also offers a working model that incorporates the important effect of pH on dithionite degradation rates in anoxic systems. Although other research to support field deployments has noted the effect of pH on dithionite lifetime, they have not incorporated this effect into a rate law to accurately predict dithionite degradation through time.

2. Materials and methods

2.1. Sample preparation

Experiments involved determination of the concentrations of dithionite and its decomposition products in solutions contained in sealed 10 mL glass ampoules. Considering that the typical pH observed in the solutions of treated aquifers ranges from 7 to 10, experiments were performed in three types of solutions: 1) 0.1 M sodium bicarbonate (Certified ACS, Fisher scientific; pH = 7.8–8.3), hereafter referred to as the HCO_3^- buffered solutions, 2) 1 wt% ethylenediaminetetraacetic acid, disodium salt dehydrate, 0.6 wt% potassium carbonate, 0.5 wt% potassium hydroxide, and 0.4 wt% potassium borate (pH = 9.8–10; Fisher Scientific pH 10 buffer solution), hereafter referred to as the EDTA/OH^- buffered solutions, and 3) in pH-unbuffered deionized water. Dithionite solutions were prepared by dissolving $Na_2S_2O_4$ (Laboratory Grade, Fisher Scientific) in the above solutions. Experiments were performed at room temperature (25 °C) with solutions having three initial concentrations of dithionite, 0.1 M, 0.05 M, 0.025 M, which were chosen to encompass the range of concentrations used in previous field injections (Istok et al., 1999; Fruchter et al., 1999). Prior to addition of dithionite salt, all solutions were degassed under vacuum and thereafter intensively purged with Ar gas to remove any traces of oxygen. Solutions were transferred via syringe into Ar-purged glass ampules. The ampules were immediately flame sealed to prevent oxygen intrusion into the solutions and potential losses of H_2S out of them. A cloudy appearance was observed in the unbuffered 0.05 M and 0.025 M solutions, which disappeared in less than one day. All glass ampules used in the study were filled the same day (total of 108 ampoules) and left undisturbed until sampled. Sampling of the solutions was performed after 1, 3, 7, 10, 14, 29, 45, 55, 66, 78, 86, and 105 days from the beginning of the experiment. Each sampling involved opening of 9 ampoules (0.1 M, 0.05 M, 0.025 M/HCO_3^- buffered solutions, EDTA/OH^- buffered solutions, unbuffered) and determination of S species and pH. Sampling was performed immediately after opening the ampoule, and analyses for all analytes were conducted as quickly as possible (approximately 5 min).

2.2. Sample analyses

For each sampling event, solutions were analyzed for concentrations of dithionite, sulfide, sulfite, thiosulfate, and sulfate. We also determined pH and, to control the mass balance of sulfur, total concentration of sulfur species able to interact with iodine (dithionite, sulfide, sulfite, thiosulfate, and polythionates, except $S_2O_6^{2-}$).

2.2.1. UV–vis analysis: $S_2O_4^{2-}$, SO_3^{2-}

When a vial was broken for sampling, an aliquot was immediately taken for UV–vis analysis (dithionite, sulfite, and thiosulfate) on a Shimadzu UV-2600 spectrophotometer. UV–vis spectra of experimental solutions were recorded in a flow-through cuvette under strictly oxygen-free conditions for the wavelengths ranging from 190 to 400 nm with an increment of 1 nm. A glass vial, containing 50 mL distilled water and 1 mL of 0.1 M HCO_3^-, which was continuously purged with Ar, was connected with tygon tubing to the cuvette. Continuous circulation of the solution between the vial and the cuvette was forced by peristaltic pump.

Dithionite concentrations were measured at a wavelength of 350 nm (Ammonette et al., 1994). Sulfite was determined at a wavelength of 200 nm. Although the $S_2O_3^{2-}$ and SO_3^{2-} UV–vis spectra overlap, both deconvolution of the UV–vis spectra and titration with formaldehyde described below indicated negligible thiosulfate formation. Owing to the near-immediate partial degradation of dithionite, calibrating the UV–vis spectral signal of dithionite-bearing solutions is essential, yet non-trivial. Known amounts of dithionite salt were added to glass vials pre-purged with Ar gas and sealed with rubber stoppers. The buffer solutions were then added by syringe through the rubber stoppers. Upon complete dissolution of the salt, an aliquot was extracted by syringe and UV–vis spectra were recorded. Another aliquot was taken for iodometric titration to determine dissolved sulfur species as described below. The latter indicated that ~50% of the dithionite underwent immediate decomposition.

2.2.2. Iodimetric titration

Another aliquot of sample was taken for iodometric titration, which determines total reduced sulfur species (Danehy and Zubritsky, 1974; Szekeres, 1974; Migdisov and Bychkov, 1998). This technique was used to determine a mass balance as it measures the concentration of all S species except oxidized S (i.e., SO_4^{2-}), elemental S, and $S_2O_6^{2-}$. In some selected samples, $S_2O_3^{2-}$ was also determined through iodometric titration with formaldehyde (Danehy and Zubritsky, 1974; Szekeres, 1974), but these analyses determined that thiosulfate formation was negligible.

The concentrations of dissolved sulfide sulfur (H_2S, HS^-) in the solutions were determined by precipitation with Cd acetate and iodometric back titration. The technique involves precipitation of sulfide sulfur in the form of insoluble CdS (by adding an aliquot of Cd acetate), separation of the precipitate from the solution by centrifuging or filtration, and the aforementioned iodometric back titration of the solid precipitate in an aliquot having an excess of HCl and iodine by sodium thiosulfate (Szekeres, 1974).

2.2.3. Ion chromatography (SO_4^{2-})

Oxidized S (i.e., SO_4^{2-} analysis) was determined on a Dionex ICS-2100 Ion Chromatography System. The aliquots which were not analyzed immediately after sampling, were immediately frozen to stop decomposition of dithionite and preclude continuous accumulation of decomposition products.

Any S in excess of the independently determined $S_2O_4^{2-}$, SO_3^{2-}, HS^-, SO_4^{2-} and $S_2O_3^{2-}$ can be attributed to zero valent sulfur, some of the polythionate species, and/or elemental sulfur involved in polysulfane chains.

2.3. Kinetics of dithionite decomposition

A numerical model was formulated to quantify the kinetics of dithionite degradation in the HCO_3^- and EDTA/OH^- buffered experiments. The unbuffered experiments were not modeled because degradation was so rapid that it was considered impractical to consider using dithionite without buffering. No attempt was made to model the very rapid initial degradation of dithionite. To allow for quantitative comparison of the HCO_3^- and EDTA/OH^- buffered experiments, a kinetic model was developed based upon the experimentally deduced stoichiometry (Equation (4) in Section 4.1) for both sets of experiments. The kinetic rate expression assumed first order dependence on dithionite concentration and a fractional order dependence on proton activity:

$$\frac{dC_i}{dt} = S_i k\{H^+\}^{\propto}\{S_2O_4^{2-}\} \quad (2)$$

where C_i is the concentration at each time step and S_i is the stoichiometric coefficient of the i^{th} chemical component in Equation (4), t is time (s), k is the kinetic rate constant, $\propto$ is a fractional exponent, and $\{S_2O_4^{2-}\}$ and $\{H^+\}$ are the respective dithionite and proton activities at

Table 2
Secondary species with corresponding mass action laws and equilibrium constants (K) used in the numerical model.

Secondary species	Mass action law	K
OH^-	$OH^- + H^+ \leftrightarrow H_2O$	$10^{14.0}$
CO_3^{2-}	$CO_3^{2-} + H^+ \leftrightarrow HCO_3^-$	$10^{10.3}$
$CO_2(aq)$	$CO_2(aq) + H_2O \leftrightarrow H^+ + HCO_3^-$	$10^{-6.34}$
HSO_3^-	$HSO_3^- \leftrightarrow H^+ + SO3^{2-}$	$10^{-7.21}$
$H_2SO_3(aq)$	$H_2SO_3(aq) \leftrightarrow 2H^+ + SO3^{2-}$	$10^{-9.21}$
HSO_4^-	$HSO_4^- \leftrightarrow H^+ + SO_4^{2-}$	$10^{-1.98}$
$H_2SO_4(aq)$	$H_2SO_4(aq) \leftrightarrow 2H^+ + SO_4^{2-}$	$10^{1.02}$
$NaCO_3^-$	$NaCO_3^- + H^+ \leftrightarrow HCO_3^- + Na^+$	$10^{9.81}$
$NaHCO_3(aq)$	$NaHCO_3(aq) \leftrightarrow HCO_3^- + Na^+$	$10^{-0.154}$
$NaOH(aq)$	$NaOH(aq) + H^+ \leftrightarrow H_2O + Na^+$	$10^{14.8}$
$NaSO_4^-$	$NaSO_4^- \leftrightarrow SO_4^{2-} + Na^+$	$10^{-0.820}$
$H_2S(aq)$	$H_2S(aq) \leftrightarrow H^+ + HS^-$	$10^{-6.99}$

each time step. The inclusion of a fractional order dependence on proton activity reflects an autocatalytic process in which there is no additional generation or consumption of protons beyond that described in Equation (4). Na^+ is also included in the model, along with HCO_3^- as a representative buffer. It was assumed that $S_2O_4^{2-}$, H_2O, SO_3^{2-}, HS^-, SO_4^{2-}, H^+, Na^+, and HCO_3^- could be modeled as total components (Benjamin, 2014) in order to include equilibrium reactions with secondary species dictated by the laws of mass action. This approach allows for a more accurate calculation of proton activity. The model includes the secondary species and corresponding mass action laws shown in Table 2, which are taken from the EQ3/6 database (Wolery, 1992). As mentioned in Section I, sulfur possesses many oxidation states and intermediate species that can form in aqueous solutions. Rather than include all potential secondary species, we focus on well-established secondary species that form in the presence of the reaction products in Equation (3) and whose equilibrium constants are readily available in the EQ3/6 thermodynamic database. Activity coefficients were calculated in each time step using the Debye-Hückel equation.

Equation (4) was coupled to Equation (2) in PFLOTRAN (Lichtner et al., 2017a,b) using its "reaction-sandbox" interface (Hammond, 2015). A model calibration procedure was used to simultaneously match the observed $S_2O_4^{2-}$ concentrations and pH trends at all three starting dithionite concentrations in both the HCO_3^- and EDTA/OH^- buffered experiments. The adjustable parameters were k and ∝. Additionally, because the reactions that occurred during the early re-equilibration phase were very complex and too rapid to be quantified from the limited number of samples that could be obtained from the sealed sacrificial reactors, the early dithionite concentrations and pH values were treated as adjustable parameters that effectively match the early observations very well. The model does not account for the early rapid degradation of dithionite, which clearly gives rise to additional species in solution that alter buffering capacity. The primary consideration was to accurately match the observed pH trends so that the pH dependence of the dithionite degradation rate could be properly described via the fitted ∝ parameter. Finally, an additional parameter needed to match the observed pH trends was the effective buffering capacity of the solutions, which was incorporated into the model as an equivalent concentration of initial bicarbonate ($[HCO_3^-]_{eff}$) for each set of experiments. Although the inclusion of an adjustable effective

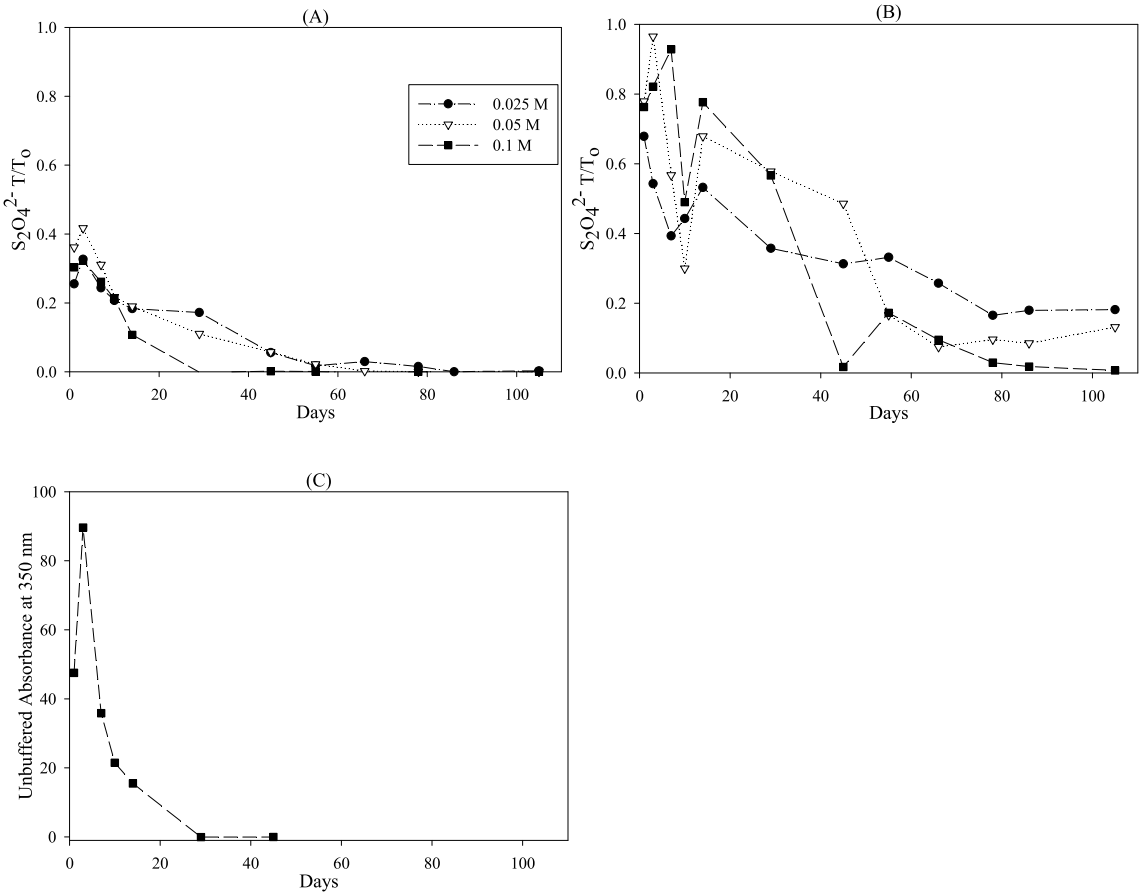

Fig. 1. Dithionite decomposition through time in (A) HCO_3^-, (B) EDTA/OH^-, and (C) unbuffered solutions. A and B show the fraction of dithionite remaining relative to starting concentrations. Absorbances are reported for the unbuffered solutions (C) as no calibration was possible owing to the rapid degradation. Data are also reported in Appendix A.1.

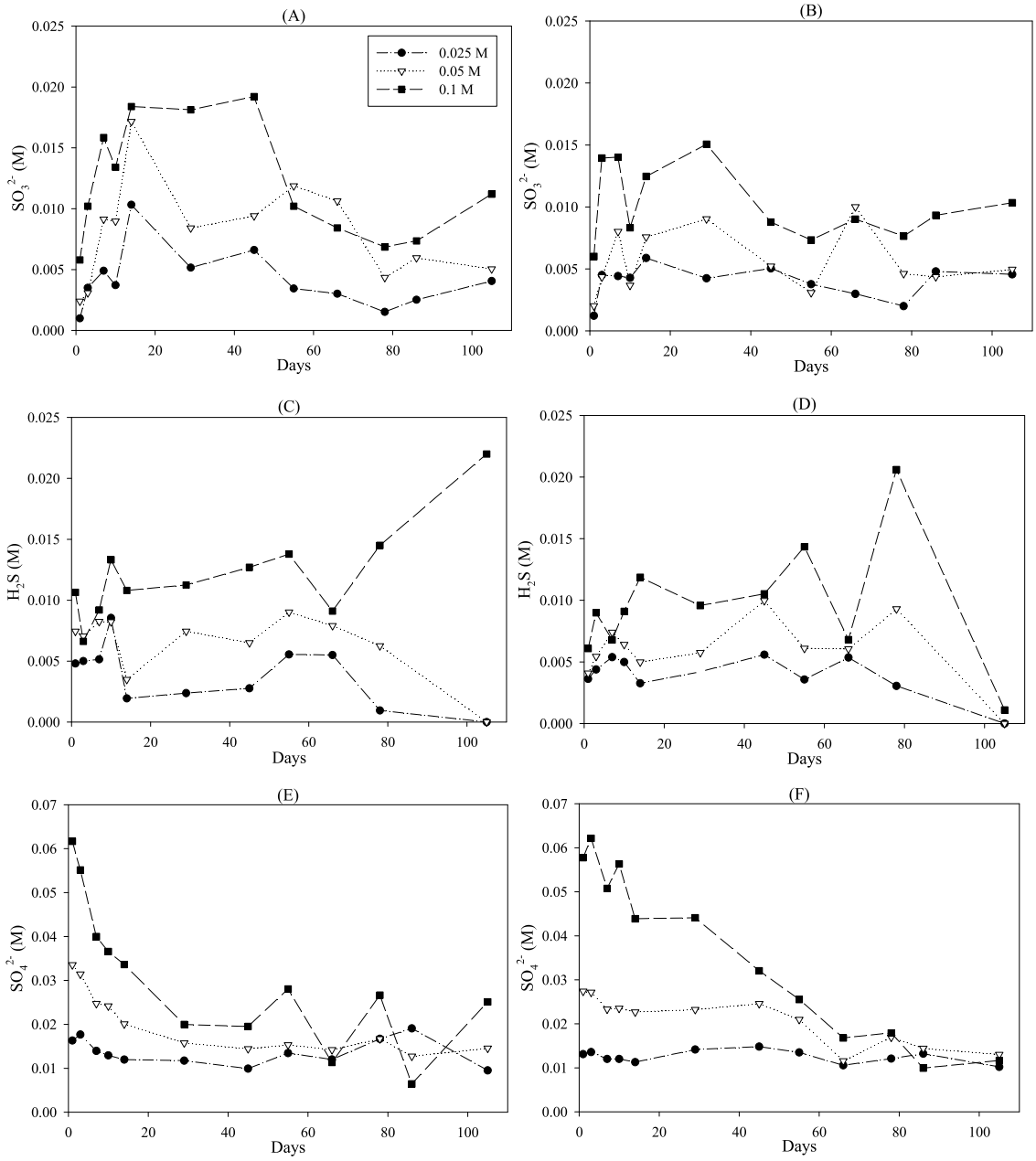

Fig. 2. Concentrations of (A, B) SO_3^{2-}, (C, D) H_2S, and (E, F) SO_4^{2-} through time in (A, C, E) HCO_3^- buffered and (B, D, F) EDTA/OH^- buffered solutions. Concentrations are also reported in Appendix A.2, A.3.

buffering capacity is a gross simplification of potentially complex equilibrium reactions involving H^+, it is consistent with treating the initial dithionite concentrations and pH as adjustable parameters, as these are all measures taken to compensate for a lack of information available to explicitly account for early reaction processes, and in the case of the EDTA/OH− buffered experiments, also the inability to explicitly account for the complexity of the added buffer. For the purposes of this study, the use of an adjustable buffering capacity allowed for more accurate prediction of pH trends, which is required for the parameterization of a pH dependent kinetic rate law. Calibration was achieved using the open-source code MADS (Vesselinov and Harp, 2012). The model parameters were calibrated using inverse analysis (utilizing Levenberg-Marquardt optimization) to reproduce the experimental observations as defined in the MADS problem setup. For a more detailed description of the PFLOTRAN-MADS calibration procedure, please refer to Appendix B.

3. Results

3.1. Dithionite concentrations through time

Concentrations of dithionite, its hydrolysis products, and pH of the solutions determined during the experiments are reported Figs. 1–3. Fig. 1 shows the decomposition of dithionite through time. The first measurement was taken 1 day after solutions were prepared. At this stage, determined concentrations of dithionite represented only a fraction of dithionite initially placed in the solution. This fraction systematically decreases with decreasing pH. For example, for HCO_3^- buffered solutions (pH = 7.5 to 7.1), recovery of dithionite after 1 day was 26–30% of the initial concentrations (Fig. 1a). Conversely, in the EDTA/OH^- buffered solutions having pH = 9.1–9.7, this value ranged from 68 to 78% (Fig. 1b). It is likely that during the first days after solution preparation dithionite undergoes complex re-equilibration

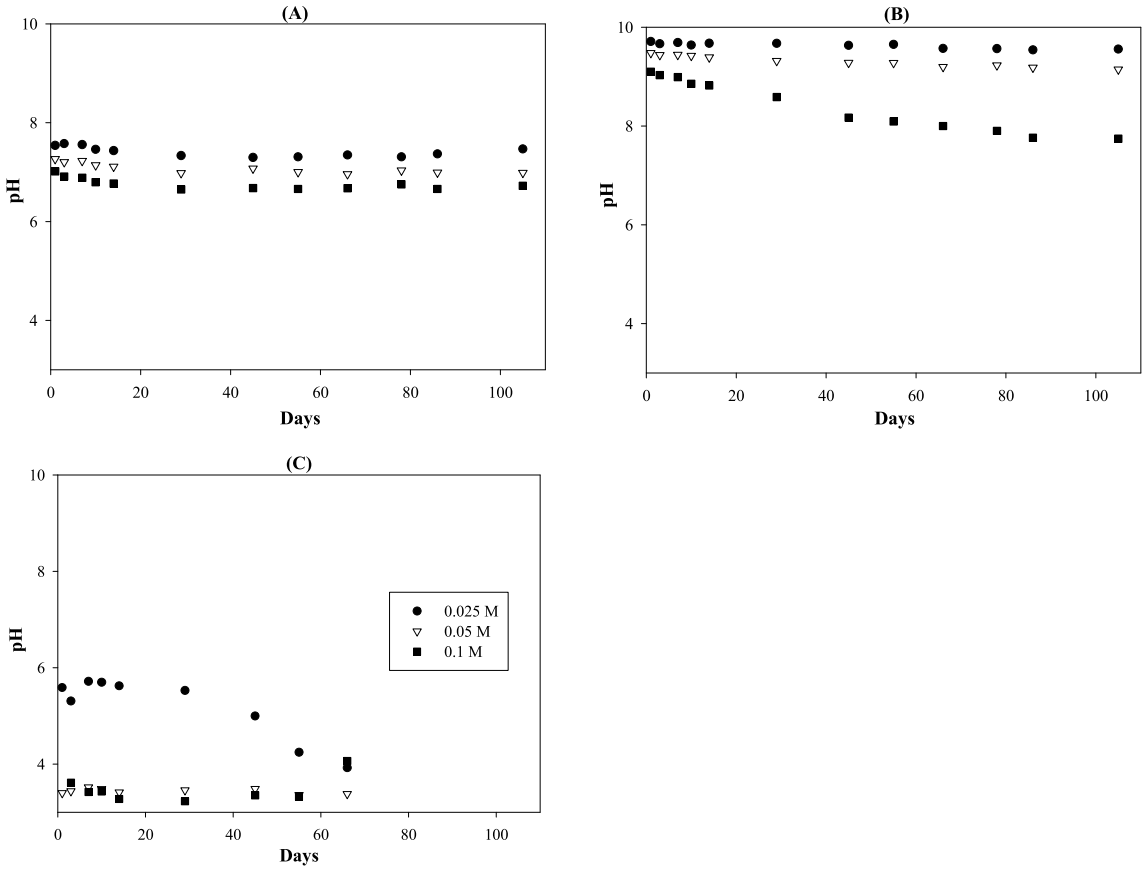

Fig. 3. pH through time in (A) HCO_3^- buffered, (B) EDTA/OH^- buffered, and (C) unbuffered solutions. pH values are also reported in Appendix A.2, A.3.

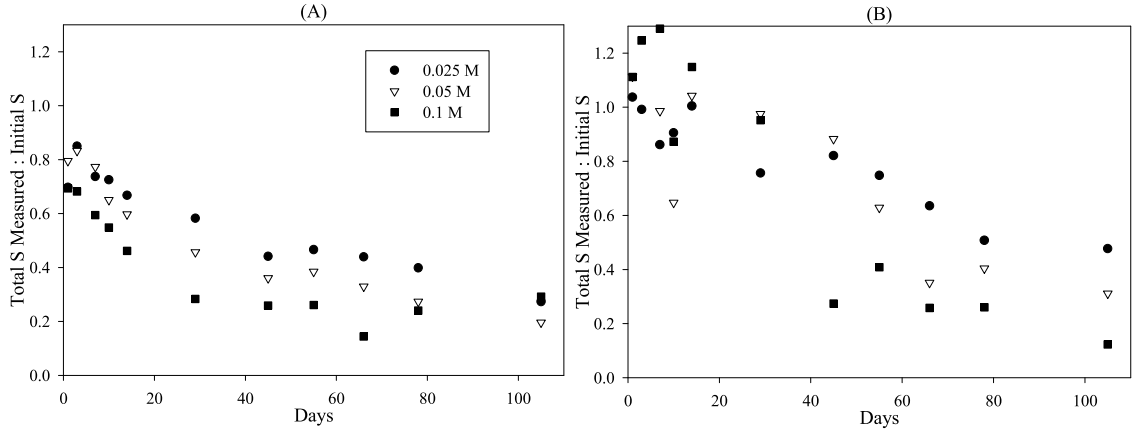

Fig. 4. Ratio of measured S relative to the starting concentration in (A) HCO_3^- buffered and (B) EDTA/OH– buffered solutions.

with its hydrolysis products: the first 3 samples taken demonstrated a relative increase of dithionite concentrations with respect to concentrations determined during day 1. The induction period and subsequent rapid autocatalytic reactions during the first few minutes of $S_2O_4^{2-}$ addition to aqueous solution have been the subject of intense study, but the current methods did not permit sampling at such frequent time intervals (Rinker et al., 1965; Burlamacchi et al., 1969; Wayman and Lem, 1970). The current study suggests that dithionite continues a rapid equilibration process over the time scale of a day or so, after which the dithionite undergoes a slow irreversible degradation until all the dithionite disappears (30 + days). Once the dithionite is gone, the reaction products presumably continue to interact with each other until a final geochemical and redox equilibrium is reached. The unbuffered solutions experienced rapid loss of dithionite. Although the 0.1 M solution persisted for 2–3 weeks, the 0.05 M and 0.025 M solutions had no measureable dithionite after the first day (Fig. 1c). Because of the rapid loss of dithionite in the unbuffered solutions, it would be impractical to consider an unbuffered dithionite deployment, so the remainder of this paper focuses on the behavior of dithionite in the buffered solutions. For the solutions buffered in HCO_3^-, dithionite disappeared after 29 days in the 0.1 M solution, whereas the disappearance was 55 and 78 days in the 0.05 M and 0.025 M solutions, respectively (Fig. 1a). Similarly, the solutions buffered with EDTA/OH^- experienced more rapid loss for the 0.1 M solution than the 0.05 and 0.025 M solutions. However, dithionite persisted much longer in all of the EDTA/OH^- buffered solutions as compared to the HCO_3^- buffered solutions, lasting until 105 days in the 0.1 M solution, and remaining present until the end of the experiment (105 days; Fig. 1b) in

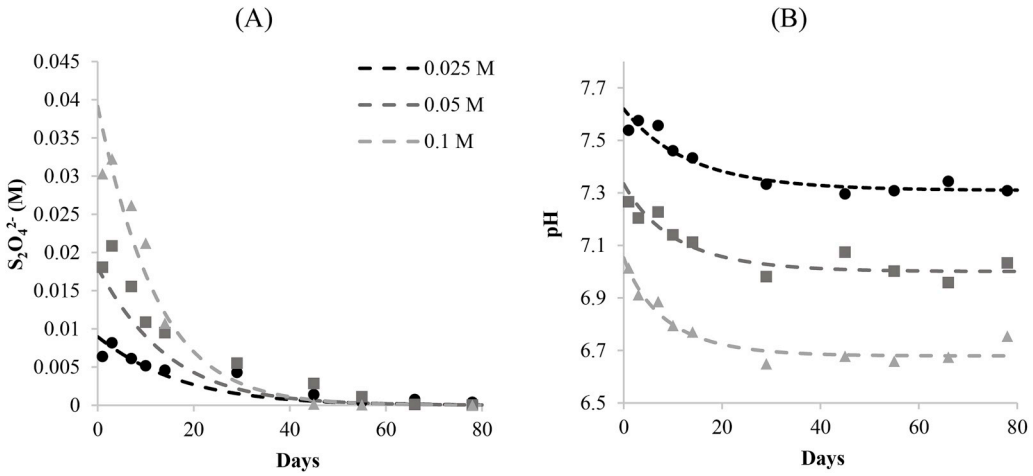

Fig. 5. Simulation of experiments conducted in the HCO_3^- buffered solution. Panel (A) shows the dithionite concentration, and Panel (B) shows pH. The figure compares calibrated model curves (dashed lines) and experimental data (points) for the different concentrations of dithionite used in these experiments.

the 0.05 and 0.025 M solutions.

3.2. Degradation products of dithionite through time

The hydrolysis products determined in the experiments demonstrate distinctively different behavior. Sulfite (SO_3^{2-}) and sulfide (HS^-) are found in nearly equimolar concentrations in effectively all sampled solutions (Fig. 2a–d; Appendix A.2, A.3). Both of these species do not show a definitive variation with time. The large temporal variability of the concentrations of SO_3^{2-} may be due, in part, to experimental errors. In order to prevent saturating the UV-detector, a very small amount of sample (0.05 mL) was diluted substantially (1210 times). The accuracy of the syringe is 0.01 mL, and thus the error with the SO_3^{2-} measurements may be as high as 20%. However, it is apparent that in all samples, the SO_3^{2-} concentrations experience an initial increase similar to that of $S_2O_4^{2-}$. Sulfite in the HCO_3^- buffered samples then appears to plateau before dropping off at around 50–60 days (Fig. 2a). Sulfite in the EDTA/OH^- buffered samples, however, decreases around 30 days but then increase by the end of the experiment (Fig. 2b). Sulfite accounts for between 2 and 12% of the total S in EDTA/OH^- buffered solutions and between 3 and 20% in HCO_3^- buffered solutions.

In HCO_3^- buffered solutions, the concentration of SO_4^{2-} decreases with time (Fig. 2e). In the first 2 samples, SO_4^{2-} accounts for about 33% of total S, but by the completion of the experiment accounts for between 5 and 20%. A similar pattern is seen with the 0.1 M sample in EDTA/OH^- buffered solution, in which the percentage of SO_4^{2-} accounting for total S drops from 33% to 5%. However, the 0.05 and 0.025 M solutions have relatively steady SO_4^{2-} concentrations through time (Fig. 2f).

In all samples, the pH decreases through time, and the decrease is more pronounced with increasing concentrations for the HCO_3^- buffered and EDTA/OH^- solutions, whereas the pH of the 0.1 M unbuffered solution is higher than either the 0.05 M or 0.025 M unbuffered solutions (Fig. 3). More specifically, in the HCO_3^- buffered solutions, the pH drops from 7.5 to 7.3 in the 0.025 M solution, from 7.3 to 7.0 in the 0.05 M solution, and from 7.0 to 6.8 in the 0.1 M solution (Fig. 3a). Similarly, in the EDTA/OH^- buffered solution, the pH drops from 9.7 to 9.6 in the 0.025 M solution, from 9.5 to 9.2 M in the 0.05 M solution and from 9.1 to 7.9 in the 0.1 M solution (Fig. 3b).

4. Discussion

4.1. Hydrolysis of dithionite

Faster degradation of dithionite at lower pH is consistent with previous studies (Lister and Garvie, 1959; Kilroy, 1980; Ammonette et al., 1994). However, accounting for all previously reported major degradation products (i.e., SO_3^{2-}, $S_2O_3^{2-}$) (Lister and Garvie, 1959; Münchow and Steudel, 1994; de Carvalho and Schwedt, 2001, 2005) in these experiments demonstrates that a substantial proportion of sulfur cannot be accounted for in near-neutral solutions (pH = 7.5 to 7.1). The sum of the S species determined in these experiments was only 68–78% of the initial total sulfur concentrations right at the first day of the experiments and demonstrated continuous decrease with time (Fig. 4a). At alkaline conditions (pH = 9.0–9.7), measured sulfur species accounted for almost 100% of initial total sulfur concentrations during the first 30 days of the experiment (Fig. 4b). Based on the analytical techniques used, the experiments were unable to account for all S species, in particular, zero-valent sulfur, some of the polythionate species, and/or elemental sulfur involved in polysulfane chains. The initial unbuffered solutions became milky white, suggesting the formation of colloidal S at low pH (~4), and other experiments have also suggested the formation of elemental S during the decomposition of dithionite (Rinker et al., 1965; Wayman and Lem, 1970; de Carvalho and Schwedt, 2001). de Carvalho and Schwedt (2001) note the disappearance of elemental sulfur within 24 h, which is consistent with our observations of the unbuffered solutions.

In addition to elemental S, which appeared to be important only at very low pH (unbuffered solutions), dithionite decomposition may produce polythionates. The decomposition of polythionates produces sulfate, elemental sulfur, and hydrogen ions and is thus consistent with the analytically measured products (Meyer and Ospina, 1982; Takano, 1987; Takano et al., 1994a; Druschel et al., 2003a,b). Therefore, we hypothesize that in these solutions formation of polythionate $S_4O_6^{2-}$ has occurred, and that the hydrolysis reaction of dithionite can be expressed as follows:

$$4\ S_2O_4^{2-} + H_2O \rightarrow HS^- + SO_3^{2-} + 2\ SO_4^{2-} + S_4O_6^{2-} + H^+ \quad (3)$$

This reaction progresses to a lesser extent as pH increases, consistent with polythionates having greater stability at low pH and undergoing decomposition at higher pH (Meyer and Ospina, 1982; Druschel et al., 2003a,b). Reaction 3 therefore is a proxy for the more rapid process of dithionite degradation observed at near-neutral pH (HCO_3^- buffered solutions). The stoichiometry of reaction 3 accounts for the initial production of protons and polythionates (i.e., unaccounted for sulfur

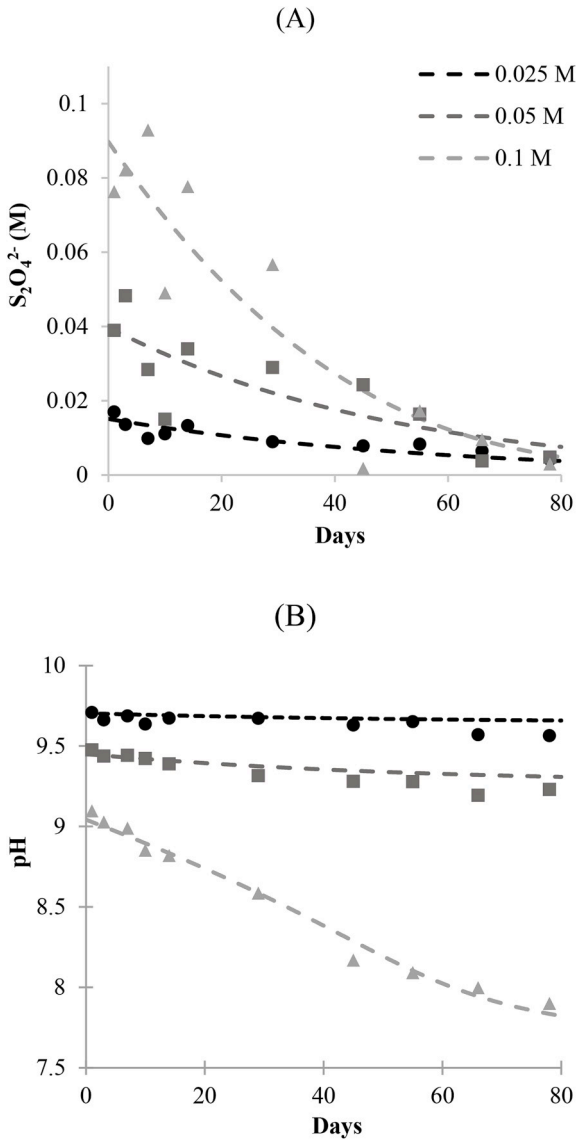

Fig. 6. Simulation of experiments conducted in the EDTA/OH^- buffered solution. Panel (A) shows the dithionite concentration, and Panel (B) shows pH. The figure compares calibrated model curves (dashed lines) and experimental data (points) for the different concentrations of dithionite used in these experiments. The fitted model parameters, k and ∝ of equation (4), are identical for the model curves of Figs. 5 and 6.

Table 3
Additional calibrated parameters used in the numerical model.

Parameter	Units	pH 8.3	pH 10
pH_i, 0.1 M $S_2O_4^{-2}$	–	7.15	9.14
pH_i, 0.05 M $S_2O_4^{-2}$	–	7.43	9.55
pH_i, 0.025 M $S_2O_4^{-2}$	–	7.71	9.81
$[S_2O_4^{-2}]_i$, 0.1 M $S_2O_4^{-2}$	M	0.0391	0.0897
$[S_2O_4^{-2}]_i$, 0.05 M $S_2O_4^{-2}$	M	0.0180	0.0397
$[S_2O_4^{-2}]_i$, 0.025 M $S_2O_4^{-2}$	M	0.00897	0.0151
$[HCO_3^-]_{eff}$	M	0.329	0.570

species) observed in HCO_3^- buffered experiments at each dithionite concentration. Because we were not able to directly measure the various polythionates and elemental sulfur, it is possible that the $S_4O_6^{2-}$ term represents the summation of other unaccounted for S species. Nevertheless, at higher pH values (EDTA/OH^- buffered solutions) and on longer time scales, this term becomes less important and the reaction is better represented as:

$$3\ S_2O_4^{2-} + 3\ H_2O \rightarrow 2HS^- + SO_3^{2-} + 3\ SO_4^{2-} + 4\ H^+ \quad (4)$$

4.2. Kinetics of dithionite decomposition

Equation (5) shows the parameterized kinetic rate law

$$\frac{dC_i}{dt} = S_i 10^{-4.81}\{H^+\}^{0.24}\{S_2O_4^{2-}\}, \quad (5)$$

where $\frac{dC_i}{dt}$ has units of mol L^{-1} s^{-1}. Results of model calibration are shown in Figs. 5 and 6, and additional calibrated model parameters for the two sets of experiments are shown in Table 3 (note that although the initial pH and initial $[S_2O_4^{2-}]$ in each experiment were technically "calibrated", the model effectively just matched these parameters to their observed values after the initial rapid equilibration period). In general, the kinetic rate model with equilibrium speciation was capable of fitting the $[S_2O_4^{2-}]$ and pH data simultaneously for all initial $S_2O_4^{2-}$ concentrations in both the HCO_3^- buffered and EDTA/OH^- buffered experiments. $[HCO_3^-]_{eff}$ for the HCO_3^- buffered solutions (0.329 M) was found to be higher than the 0.1 M HCO_3^- used, which is most likely due to the early rapid generation of reaction products that have buffering capacity (e.g. $H_2S_4O_6$(aq), $HS_4O_6^-$) not considered in the model. The high calibrated value of $[HCO_3^-]_{eff}$ for the EDTA/OH^- buffered experiments (0.570 M) was likely due to the complex buffers used in stock buffer solution.

Equation (5) was used to estimate half-lives of each experiment by treating $10^{-4.81}\{H^+\}_i^{0.24}$ as a pseudo first order rate constant, where $\{H^+\}_i$ is the initial proton activity calculated using the calibrated value of pH_i, and normalizing by the stoichiometric coefficient of $S_2O_4^{2-}$ in Equation (4). The estimated half-lives for the HCO_3^- buffered experiments were 9.06, 10.6, and 12.4 days for the 0.1, 0.05, and 0.025 M dithionite concentrations, respectively, resulting in a mean half-life of 10.7 days. The estimated half-lives for the EDTA/OH^- buffered experiments were 27.2, 34.2, and 39.5 days for 0.1 M, 0.05 M, and 0.025 M dithionite concentrations respectively, resulting in a mean half-life of 33.6 days. The mean values represent single best estimates that consider all initial starting concentrations for a given pH while also assuming that the half-life varies with pH but not dithionite concentration (pseudo first-order). The longer half-life reported at the higher pH in the present study relative to the half-lives reported by Amonette et al. (1994) at a similar pH is most likely the result of preventing any gases from either entering or leaving the glass-sealed ampoules in the current study. It is well known that oxygen reacts rapidly with dithionite (Rinker et al., 1960; Creutz and Sutin, 1974), and care was taken in both studies to minimize or eliminate oxygen, but the present study also prevented the egress of gasses from the reaction vessels. Amonette et al. (1994) do not mention any measures taken to prevent H_2S egress (which can occur through many types of vessel caps or stoppers), and we hypothesize that keeping the H_2S in our reaction vessels slowed the degradation of dithionite because it maintained a higher concentration of the degradation product(s) HS^-/S^{2-} in solution.

Although the rate law (equation (5)) can effectively predict the post-rapid-hydrolysis degradation rate as a function of pH, several lines of evidence suggest that assuming reaction (4) accounts for all dithionite degradation and using only the limited assemblage of species and reactions in Table 2 greatly oversimplifies the system. The fact that the pH trends in the experiments can only be matched if the initial effective pH buffering of the system (the first ~ 3 days) is treated as an adjustable parameter is one such line of evidence. Also, as $S_2O_4^{2-}$ concentrations decrease with time, the concentrations of reaction (4) products SO_4^{2-}, SO_3^{2-} and HS^- measured in the experiments either decreased or stayed relatively constant. This is contrary to simulation results. These species are reaction products in reaction (4), so the model predicted that their concentration would increase proportionally to the amount of dithionite that is degraded. Instead, it is the concentration(s)

of the unaccounted for reduced S species, which are not considered in the model, that consistently increase with time. These observations suggest that (1) there are unaccounted-for reaction products that are involved in hydrolysis and acid-base reactions that are not considered by the model, and (2) the sulfur chemistry evolves in a complex manner as a result of interactions between reduced and oxidized sulfur reaction products that are not thermodynamically compatible.

4.3. Implications for environmental remediation

As a strong reducing agent, dithionite has the potential to be a useful chemical for environmental remediation of oxic contaminants, such as Cr(VI). However, its high reactivity makes it challenging to deploy in the field, and even if oxygen is eliminated from solution before addition, dithionite degradation still occurs at a significant rate. The results of this study suggest that in order to develop a complete mechanistic model of dithionite degradation, simultaneous determination of every S species on the time scale of minutes would be required. However, we reasoned that the early-time degradation behavior of dithionite, other than the fraction of dithionite remaining, is not of practical importance because this rapid degradation will occur almost immediately upon dissolving dithionite. Thus, we focused on the development of a semi-mechanistic, semi-empirical rate law describing anoxic aqueous decomposition of dithionite as a function of pH *after* the initial rapid degradation/equilibration process. Although we did not address dithionite decomposition in the presence of oxygen or aquifer sediments, knowledge of anaerobic decomposition rates should prove valuable for such follow-on studies because anoxic decomposition will always be superimposed on oxic decomposition. From a practical standpoint, the anoxic conditions of this study are relevant for estimating how far into an aquifer dithionite can be "pushed" from an injection well. Assuming dithionite reacts rapidly with any dissolved oxygen and oxidized sediments that are present in the aquifer (e.g., ferric and manganese oxides), these oxic reactants will eventually be consumed in the vicinity of an injection well, and if dithionite is continuously injected, the distance that it can ultimately be pushed into an aquifer will be dictated by its anaerobic decomposition rate in the presence of aqueous phase reaction products.

It was determined that ~70% of dithionite hydrolyzes almost immediately in a HCO_3^- buffered anoxic system and about 20% hydrolyzes immediately in an anoxic solution buffered to pH ~9.5. However, in both cases, the decomposition of the remaining dithionite is much slower, with dithionite concentrations remaining measurable for over 50 and 100 days, respectively. This observation has important implications for field deployments, namely that loss of dithionite due to anoxic decomposition occurs more slowly than previously thought. The half-lives reported here are 2 times longer than those reported by Ammonette et al. (1994) for comparable pHs and dithionite concentrations, which we attribute to keeping volatile reaction products, such as H_2S gas, from escaping from the reactors. Such volatile reaction products should also remain in solution in confined aquifers, particularly when an overpressure is imposed to inject a dithionite solution at a reasonable rate. This implies that in an ideal system of radial flow near an injection well (penetration distance into aquifer proportional to square root of time), dithionite can be effectively injected $\sqrt{2}$ times further into an aquifer than previously thought for a given injection flow rate. Consequently, the spacing of injection wells for establishing an in-situ barrier can be increased, which can translate to significant cost savings, particularly in deep, contaminated aquifers, such as those in Los Alamos.

Acknowledgements

The authors would like to acknowledge David Chu for ion chromatography analysis of sulfate. This work was funded by the U.S. Department of Energy Office of Environmental Management and Environmental Programs (ADEP) at Los Alamos National Laboratory.

Appendix A. Supplementary data

Supplementary data to this article can be found online at https://doi.org/10.1016/j.apgeochem.2018.12.015.

References

Amonette, J.E., Szecsody, J.E., Schaef, H.T., Templeton, J.C., Gorby, Y.A., Fruchter, J.S., 1994. Abiotic Reduction of Aquifer Materials by Dithionite: a Promising In-situ Remediation Technology. Pacific Northwest Lab., Richland, WA (United States) No. PNL-SA_24505; CONF-941124022.

Benjamin, M.M., 2014. Water Chemistry. Waveland Press, Illinois.

Boparai, H.K., Comfort, S.D., Shea, P.J., Szecsody, J.E., 2008. Remediating explosive-contaminated groundwater by in situ redox manipulation (ISRM) of aquifer sediments. Chemosphere 71 (5), 933–941.

Burlamacchi, L., Guarini, G., Tiezzi, E., 1969. Mechanism of decomposition of sodium dithionite in aqueous solution. Trans. Faraday Soc. 65, 496–502.

Burton, E.D., Bush, R.T., Johnston, S.G., Sullivan, L.A., Keene, A.F., 2011. Sulfur biogeochemical cycling and novel Fe-S mineralization pathways in a tidally re-flooded wetland. Geochem. Cosmochim. Acta 75 (12), 3434–3451.

Casas, A.S., Armienta, M.A., Ramos, S., 2016. Sulfur speciation with high performance liquid chromatography as a tool for El Chichón volcano, crater lake monitoring. J. South Am. Earth Sci. 72, 241–249.

Couture, R.M., Fischer, R., Van Cappellen, P., Gobeil, C., 2016. Non-steady state diagenesis of organic and inorganic sulfur in lake sediments. Geochem. Cosmochim. Acta 194, 15–33.

Creutz, C., Sutin, N., 1974. Kinetics of the reactions of sodium dithionite with dioxygen and hydrogen peroxide. Inorg. Chem. 13 (8), 2041–2043.

Danehy, J.P., Zubritsky, C.W., 1974. Iodometric method for the determination of dithionite, bisulfite, and thiosulfate in the presence of each other and its use in following the decomposition of aqueous solutions of sodium dithionite. Anal. Chem. 46 (3), 391–395.

de Carvalho, L.M., Schwedt, G., 2001. Polarographic determination of dithionite and its decomposition products: kinetic aspects, stabilizers, and analytical application. Anal. Chim. Acta 436 (2), 293–300.

de Carvalho, L.M., Schwedt, G., 2005. Sulfur speciation by capillary zone electrophoresis Determination of dithionite and its decomposition products sulfite, sulfate and thiosulfate in commercial bleaching agents. J. Chromatogr. A 1099 (1), 185–190.

Druschel, G.K., Hamers, R.J., Banfield, J.F., 2003a. Kinetics and mechanism of polythionate oxidation to sulfate at low pH by O2 and Fe3 + . Geochem. Cosmochim. Acta 67 (23), 4457–4469.

Druschel, G.K., Hamers, R.J., Luther, G.W., Banfield, J.F., 2003b. Kinetics and mechanism of trithionate and tetrathionate oxidation at low pH by hydroxyl radicals. Aquat. Geochem. 9 (2), 145–164.

Fruchter, J.S., Cole, C.R., Williams, M.D., Vermeul, V.R., Amonette, J.E., Szecsody, J.E., Istok, J.D., Humphrey, M.D., 1999. Creation of a subsurface permeable treatment zone for aqueous chromate contamination using in situ redox manipulation. Groundwater Monit. Rem. 20 (2), 66–77.

Hammond, G.E., 2015. PFLOTRAN: recent developments facilitating massively-parallel reactive biogeochemical transport. In: AGU Fall Meeting. American Geophysical Union Fall Meeting 2015.

Holman, D.A., Bennett, D.W., 1994. A multicomponent kinetics study of the anaerobic decomposition of aqueous sodium dithionite. J. Phys. Chem. 98 (50), 13300–13307.

Istok, J.D., Amonette, J.E., Cole, C.R., Fruchter, J.S., Humphrey, M.D., Szecsody, J.E., Teel, S.S., Vermeul, V.R., Williams, M.D., Yabusaki, S.B., 1999. In situ redox manipulation by dithionite injection: intermediate-scale laboratory experiments. Ground Water 37 (6), 884–889.

Kaasalainen, H., Stefánsson, A., 2011. Sulfur speciation in natural hydrothermal waters, Iceland. Geochim. Cosmochim. Acta. 75 (10), 2777–2791.

Kaasalainen, H., Stefánsson, A., 2011. Chemical analysis of sulfur species in geothermal waters. Talanta 85 (4), 1897–1903.

Kilroy, W.P., 1980. Anaerobic decomposition of sodium dithionite in alkaline solution. J. Inorg. Nucl. Chem. 42 (7), 1071–1073.

Lem, W.J., Wayman, M., 1970. Decomposition of aqueous dithionite. Part I. Kinetics of decomposition of aqueous sodium dithionite. Can. J. Chem. 48 (5), 776–781.

Lichtner, P.C., Hammond, G.E., Lu, C., Karra, S., Bisht, G., Andre, B., Mills, R.T., Kumar, J., Frederick, J.M., 2017a. PFLOTRAN User Manual. http://www.documentation.pflotran.org.

Lichtner, P.C., Hammond, G.E., Lu, C., Karra, S., Bisht, G., Andre, B., Mills, R.T., Kumar, J., Frederick, J.M., 2017b. PFLOTRAN Webpage. http://www.pflotran.org.

Lister, M.W., Garvie, R.C., 1959. Sodium dithionite, decomposition in aqueous solution and in the solid state. Can. J. Chem. 37 (9), 1567–1574.

Ludwig, R.D., Su, C., Lee, T.R., Wilkin, R.T., Acree, S.D., Ross, R.R., Keeley, A., 2007. In situ chemical reduction of Cr(VI) in groundwater using a combination of ferrous sulfate and sodium dithionite: a field investigation. Environ. Sci. Technol. 41 (15), 5299–5305.

Luther, G.W., Church, T.M., 1998. Seasonal cycling of sulfur and iron in porewaters of a Delaware salt marsh. Mar. Chem. 23 (3–4), 295–309.

Meyer, B., Ospina, M., 1982. Raman spectrometric study of the thermal decomposition of aqueous tri- and tetrathionate. Phosphorus Sulfur Relat. Elem. 14 (1), 23–36.

Migdisov, A.A., Bychkov, A.Y., 1998. The behavior of metals and sulphur during the

formation of hydrothermal mercury—antimony—arsenic mineralization, Uzon caldera, Kamchatka, Russia. J. Volcanol. Geoth. Res. 4, 153–171.
Münchow, V., Steudel, R., 1994. The decomposition of aqueous dithionite and its reactions with polythionates SnO62- (n = 3-5) studied by ion-pair chromatography. Z. Anorg. Allg. Chem. 620 (1), 121–126.
Nzengung, V.A., Castillo, R.M., Gates, W.P., Mills, G.L., 2001. Abiotic transformation of perchloroethylene in homogeneous dithionite solution and in suspensions of dithionite-treated clay minerals. Environ. Sci. Technol. 35 (11), 2244–2251.
Rinker, R.G., Gordon, T.P., Mason, D.M., Sakaida, R.R., Corcoran, W.H., 1960. Kinetics and mechanism of the air oxidation of the dithionite ion (S2O4 =) in aqueous solution. J. Phys. Chem. 64 (5), 573–581.
Rinker, R.G., Lynn, S., Mason, D.M., Corcoran, W.H., 1965. Kinetics and mechanism of thermal decomposition of sodium dithionite in aqueous solution. Ind. Eng. Chem. Fundam. 4 (3), 282–288.
Spencer, M.S., 1967. Chemistry of sodium dithionite. Part 1.—kinetics of decomposition in aqueous bisulphite solutions. Trans. Faraday Soc. 63, 2510–2515.
Szecsody, J.E., Fruchter, J.S., Williams, m. D., Vermeul, V.R., Sklarew, D., 2004. In situ chemical reduction of aquifer sediments: enhancement of reactive iron phases and TCE dechlorination. Environ. Sci. Technol. 38 (17), 4656–4663.
Szekeres, L., 1974. Analytical chemistry of the sulfur acids. Talanta 21 (1), 1–44.
Takano, B., 1987. Correlation of volcanic activity with sulfur oxyanion speciation in a crater lake. Science 235, 1633–1636.
Takano, B., Watanuki, K., 1990. Monitoring of volcanic eruptions at Yugama crater lake by aqueous sulfur oxyanions. J. Volcanol. Geoth. Res. 40 (1), 71–87.
Takano, B., Ohsawa, S., Glover, R.B., 1994a. Surveillance of ruapehu crater lake, New Zealand, by aqueous polythionates. J. Volcanol. Geoth. Res. 60 (1), 29–57.
Takano, B., Saitoh, H., Takano, E., 1994b. Geochemical implications of subaqueous molten sulfur at Yugama crater lake, Kusatsu-Shirane volcano, Japan. Geochem. J. 28 (3), 199–216.
Vesselinov, V., Harp, D., 2012. June. Model analysis and decision support (MADS) for comple physics models. In: XIX International Conference on Water Resources-CMWR.
Wayman, M., Lem, W.J., 1970. Decomposition of aqueous dithionite. Part II. A reaction mechanism for the decomposition of aqueous sodium dithionite. Can. J. Chem. 48 (5), 782–787.
Williamson, M.A., Rimstidt, J.D., 1992. Correlation between structure and thermodynamic properties of aqueous sulfur species. Geochem. Cosmochim. Acta 56 (11), 3867–3880.
Wolery, T.J., 1992. EQ3/6: a Software Package for Geochemical Modeling of Aqueous Systems: Package Overview and Installation Guide (Version 7.0). Lawrence Livermore National Laboratory, Livermore, CA, pp. 1–65.
Xie, Y., Cwiertny, D.M., 2010. Use of dithionite to extend the reactive lifetime of nanoscale zero-valent iron treatment systems. Environ. Sci. Technol. 44 (22), 8649–8655.
Xu, Y., Schoonen, M.A.A., Nordstrom, D.K., Cunningham, K.M., Ball, J.W., 1998. Sulfur geochemistry of hydrothermal waters in Yellowstone National Park: I. The origin of thiosulfate in hot spring waters. Geochem. Cosmochim. Acta 62 (23), 3729–3743.